



Monoisotopic silver nanoparticles-based mass spectrometry imaging of human bladder cancer tissue: Biomarker discovery



Krzysztof Ossoliński^a, Tomasz Ruman^b, Tadeusz Ossoliński^a, Anna Ossolińska^a, Adrian Arendowski^b, Artur Kołodziej^{b,c}, Aneta Płaza-Altamer^{b,c}, Joanna Nizioł^{b,*}

^a Department of Urology, John Paul II Hospital, Kolbuszowa, Poland

^b Rzeszów University of Technology, Faculty of Chemistry, Rzeszów, Poland

^c Doctoral School of Engineering and Technical Sciences at the Rzeszów University of Technology, Rzeszów, Poland

ARTICLE INFO

Keywords:

Silver nanoparticles
LDI-MS
Biomarkers
Bladder cancer
Human tumor tissue

ABSTRACT

Purpose: Bladder cancer (BC) is the 10th most common form of cancer worldwide and the 2nd most common cancer of the urinary tract after prostate cancer, taking into account both incidence and prevalence.

Materials/methods: Tissues from patients with BC and also tissue extracts were analyzed by laser desorption/ionization mass spectrometry imaging (LDI-MSI) with monoisotopic silver-109 nanoparticles-enhanced target (¹⁰⁹AgNPET).

Results: Univariate and multivariate statistical analyses revealed 10 metabolites that differentiated between tumor and normal tissues from six patients with diagnosed BC. Selected metabolites are discussed in detail in relation to their mass spectrometry (MS) imaging results. The pathway analysis enabled us to link these compounds with 17 metabolic pathways.

Conclusions: According to receiver operating characteristic (ROC) analysis of biomarkers, 10 known metabolites were identified as the new potential biomarkers with areas under the curve (AUC) higher than >0.99. In both univariate and multivariate analysis, it was predicted that these compounds could serve as useful discriminators of cancerous versus normal tissue in patients diagnosed with BC.

1. Introduction

Bladder cancer (BC) is the 12th most common form of cancer worldwide and the 2nd most common cancer of the urinary tract after prostate cancer, taking into account both incidence and prevalence [1]. Globally, 573,278 new cases of BC were diagnosed in 2020. In terms of incidence, it is the 6th most common cancer in men, the 17th in women and the 10th most frequent cancer in both sexes [1]. Cystoscopic examination of bladder remains the gold standard for BC diagnosis, but it is invasive, associated with discomfort, sometimes painful and costly. It is estimated that 4–27% of tumors are omitted during the examination. This value increases to 32–77% in the case of carcinoma *in situ* (CIS) [2].

In recent years, numerous urine-based BC biomarkers have been evaluated but currently there is no reliable diagnostic and prognostic BC biomarker that has been accepted for diagnosis and follow-up in routine practice or clinical guidelines and which could be an alternative to cystoscopy. Over the past decade, due to the molecular specificity and sensitivity mass spectrometry (MS) has been used as a main technique in

biomarker discovery field [3]. Two-dimensional variety of MS – mass spectrometry imaging (MSI) plays an increasingly important role in the field of molecular imaging because it allows direct mapping of the distribution of a variety of endogenous and exogenous compounds within biological tissues with high specificity and without the need for radioactive or fluorescent radioactive labelling normally used in histochemical protocols [4]. BC tissues were studied previously with MSI techniques such as matrix-assisted laser desorption ionization (MALDI) [5] and desorption electrospray ionization (DESI) [6]. It should be noted that there are no BC MS and MSI results made with the use of nanoparticle-based methods published to date. It is important to state that nanoparticle-based methods have many advantages with regard to other methods including very efficient cationization of low molecular weight compounds, relatively high sensitivity of analyte detection, very low chemical background and high mass accuracy due to internal calibration, unlike commonly used one - MALDI. They allow for higher lateral resolutions and higher sensitivity when compared to DESI. In our recent publications we presented new methods such as gold nanoparticle-enhanced target (AuNPET) [7], silver

* Corresponding author. University of Technology, Faculty of Chemistry, 6 Powstańców Warszawy Ave., 35-959, Rzeszów, Poland.

E-mail address: jnizioł@prz.edu.pl (J. Nizioł).

<https://doi.org/10.1016/j.advms.2022.12.002>

Received 21 May 2022; Received in revised form 5 September 2022; Accepted 8 December 2022

nanoparticle-enhanced target (AgNPET) [8] and monoisotopic silver-109 nanoparticles-enhanced target ($^{109}\text{AgNPET}$) [9] with results of their application for imaging of plant, animal and human tissues [10–12].

2. Materials and methods

2.1. Participants

Cancer and normal tissue samples were collected from 6 patients (Caucasian race, average age 65 years, 2 females and 4 males) with diagnosed BC at John Paul II Hospital in Kolbuszowa (Poland). All patients underwent transurethral resection of bladder tumor (TURBT) following a detailed clinical history and laboratory examination. Each of these patients had at least an abdominal ultrasound to exclude other tumors (patients with urolithiasis usually also had a CT scan) and a basic package of laboratory tests required for urological surgery to exclude inflammation. Whole tumor and a small fragment of adjacent healthy uroepithelium were resected (cancer and control tissue). The histopathological analysis of resected tumors from all patients, confirmed non-invasive (pTa) low-grade (LG) urothelial papillary carcinoma, according to 2004 WHO grading system [13,14]. Control tissues were free of cancer cells. The clinical characteristics of the patients are presented in [Supplementary Table S1](#).

2.2. Materials and equipment

Silver-109 (min. 99.75% of ^{109}Ag) isotope was purchased from BuyIsotope (Neonest AB, Stockholm, Sweden) and transformed to trifluoroacetate salt by commonly known methods (involving dissolving in HNO_3 , precipitation of $^{109}\text{AgOH}$ and reaction with trifluoroacetic acid) and recrystallized from tetrahydrofuran/hexane system. 2,5-Dihydroxybenzoic acid (DHB) was purchased from Sigma-Aldrich (St. Louis, USA). Steel targets were locally machined from H17 stainless steel. All solvents were of high-performance liquid chromatography (HPLC) quality, except for water (18 M Ω water was produced locally) and methanol (liquid chromatography-mass spectrometry - LC MS - grade, FlukaTM, (Seelze, Germany). The silver-109 nanoparticles were synthesized on the surface of steel targets as described in our recent publication [9]. Optical photographs of tissue samples were made with the use of an Olympus SZ10 microscope equipped with an 8 MPix Olympus digital camera (Hamburg, Germany).

2.3. Preparation of monoisotopic silver suspension

Four milligrams of silver-109 trifluoroacetate ($^{109}\text{AgTFA}$) and 14 mg of DHB were quantitatively transferred to a glass tube by dissolving in 2 ml of isopropanol and 2 ml of acetonitrile. The prepared solution was placed in an ultrasonic bath set at 50 °C for about 30 min. After this time, the suspension was ready to use.

2.4. Imaging sample preparation

Tissues from 6 patients with the same tumor stage and grade were selected for LDI-MSI analysis. Three independent imaging experiments were performed to exclude possible random results, one for tissues from patient no. 1, another for patients no. 2–4 and the last for patients no. 5 and 6. The material examined was six pairs of BC and normal tissue fragments of average 3 × 3 mm size. MS imaging for patient no. 1 was carried out within about an hour after the material was collected after surgery. Until then, the tissue samples were stored at a temperature of approx. 2–4 °C. Tissues from patients no. 2–6 were stored at –60 °C and thawed to 4 °C before the MSI measurements. To remove excess liquid material, samples were touched to cellulose filter paper (3 times). Next, with the use of sterile needles and tweezers, a few imprints of the examined tissues were made on the previously prepared $^{109}\text{AgNPET}$ plate. The material was transferred from the BC patients to the

$^{109}\text{AgNPET}$ substrate by briefly touching (3 s) the tissue samples to steel surface with light pressure. Steel target with imprints was placed on a computer-controlled 3D positioning table and sprayed with nanoparticles using an electrospray ionization mass spectrometry (ESI-MS) nebulizer with nitrogen as nebulizing gas (2 bar). Target was placed in a MALDI time-of-flight MS (MALDI-ToF/ToF MS) (Autoflex Speed ToF/ToF, Bruker, Bremen, Germany) and selected imprints were then directly analyzed.

2.5. LDI-MS imaging experiments

LDI-MSI experiments were performed using a Bruker Autoflex Speed ToF/ToF mass spectrometer (MALDI ToF/ToF, Bruker, Bremen, Germany) in positive-ion reflectron mode. FlexImaging 4.0 software was used for data processing and analysis. The apparatus was equipped with a SmartBeam II 1000 Hz 355 nm laser. Laser impulse energy was approximately 100–190 μJ , laser repetition rate was 1000 Hz, and deflection was set on m/z lower than 80 Da. The m/z range was 80–2000 Da, spatial resolution 250 × 250 μm . The experiments were made with 20,000 laser shots per individual spot with a default random walk applied (random points with 50 laser shots). All spectra were calibrated with the use of silver ions ($^{109}\text{Ag}^+$ to $^{109}\text{Ag}_{10}^+$). The first accelerating voltage was held at 19 kV, and the second ion source voltage was held at 16.7 kV. Reflector voltages used were 21 kV (the first) and 9.55 kV (the second). All of the ion images were within $\pm 0.05\%$ of m/z . Total ion current (TIC) normalization was used for all results shown.

2.6. Preparation of tissue extracts

Small portions of frozen neoplastic bladder tissue ($n = 6$) and normal control tissues ($n = 6$) of approximately 2 mg each were transferred to Eppendorf tubes and then homogenized by three cycles of freezing and thawing. Next to the homogenates 500 μl of 2:1 (v/v) chloroform/methanol were added and then extracted for 30 min in ultrasonic bath (at 2–4 °C.) The tubes were centrifuged for 5 min at an acceleration of 6000 $\times g$ and the phases were allowed to separate. The water-methanol and methanol-chloroform phases were transferred to separate tubes and then methanol-chloroform phases were diluted 100x whereas the water-methanol phases were measured without dilution. Volume of 0.3 μl of each sample was placed on $^{109}\text{AgNPET}$ and allowed to dry at room temperature and target placed in a MALDI ToF/ToF MS. Tissue extracts were made to confirm the structure of the identified compounds by MS/MS measurements.

2.7. LDI-MS and MS/MS of tissue extracts

LDI-MSI experiments were performed using a Bruker Autoflex Speed MALDI ToF/ToF MS (Autoflex Speed ToF/ToF, Bruker, Bremen, Germany) in positive-ion reflectron mode. The apparatus was equipped with a SmartBeam II 1000 Hz 355 nm laser. Laser impulse energy was approximately 100–190 μJ , laser repetition rate was 1000 Hz, and deflection was set on m/z lower than 80 Da. The m/z range was 80–2000 Da. Spectrum for each extract contained data from 20k laser shots with a default random walk applied (random points with 50 laser shots). All spectra were calibrated with the use of silver ions ($^{109}\text{Ag}^+$ to $^{109}\text{Ag}_{10}^+$). The first accelerating voltage was held at 19 kV, and the second ion source voltage was held at 16.7 kV. Reflector voltages used were 21 kV (the first) and 9.55 kV (the second). MS/MS measurements were performed using the LIFT (low mass) method [15]. The mass window for precursor ion selection used was ± 0 Da. FlexAnalysis (version 4.0, Bruker, Bremen, Germany) was used for data analysis.

2.8. Data processing

The average spectra of the imprint area of cancerous and normal tissue from patient no. 1 were generated and then compared in the using

the SCIls Lab software version 2016b (SCIls, Bremen, Germany) and FlexAnalysis (version 4.0, Bruker, Bremen, Germany). Statistical analysis was performed using the Cardinal MSI (R package) [16] with hotspot suppression and Gaussian smoothing applied and MetaboAnalyst 5.0 platform [17]. Database search of chemical compounds were carried out using a custom-made program. Theoretical m/z values were calculated using ChemCalc program available online [18].

Data of peak mean abundance from the entire area of the examined cancer ($n = 6$) and control ($n = 6$) tissue were formatted as comma separated values (.csv) files and uploaded to the MetaboAnalyst 5.0 server [17]. Metabolite data was checked for data integrity and normalized using MetaboAnalyst's normalization protocols (normalization by sum, log transformation and auto-scaling), both for biomarker and pathway analyses. Univariate analysis (t -test), fold-change analysis and orthogonal partial least squares discriminant analysis (OPLS-DA) were applied to calculate the statistical significance of the metabolites between the two groups (cancer over control). To identify the potential biomarkers associated with BC, the Receiver Operating Characteristic (ROC) curve was applied using biomarker analysis module of MetaboAnalyst v 5.0. The ROC curves were generated using an algorithm based on Monte-Carlo cross validation (MCCV) through balanced subsampling coupled with linear support vector machine (SVM) for the classification method and SVM built-in for the feature ranking method. To identify the most relevant metabolic pathways involved in BC, metabolic pathway analysis was performed using MetaboAnalyst with *Homo sapiens* pathway libraries.

3. Ethical issues

The study protocol was approved by local Bioethics Committee at the University of Rzeszow, Poland (permission no. 2018/04/10) and performed in accordance with relevant guidelines and regulations, including the 1964 Helsinki declaration and its later amendments. Specimens and clinical data from patients involved in the study were collected with written consent.

4. Results and discussion

$^{109}\text{AgNPET}$ method was used previously for LDI-MS analysis of low molecular weight (LMW) compounds and biological material and was shown to be a promising alternative to traditional MALDI method [9,19]. LDI-MSI experiments were performed by measuring series of high-resolution MS spectra with $250 \times 250 \mu\text{m}$ resolution of bladder tissue imprints of ca. $3 \times 3 \text{ mm}$ size made on $^{109}\text{AgNPET}$ target plate. In order to estimate whether there is a sample-related differentiation between cancer and normal tissue imprints, a statistical analysis was performed for patient no. 1 tissue pair. Data derived from MSI experiment were analyzed by comparison of average spectra of cancer and normal areas by spatial shrunken centroids with adaptive weights (SSCA). The mentioned method allows estimation of the probability that a location of interest belongs to a particular segment and was previously used among others for segmentation of data for whole-body MALDI MSI experiment [20]. Images of the major regions of the BC tissue from patient no. 1 were outlined by SSCA segmentation as shown in Supplementary Fig. S1. What is interesting, images generated with the aid of Cardinal MSI with SSCA method are very similar to the ion images obtained in MSI experiment and suggest that: (i) areas of imprints are clearly different from target area with no fuzzy boundaries and (ii) cancerous area is clearly different from the normal one.

4.1. Identification of metabolite biomarkers

The analysis of MSI data revealed a list of 28 compounds for which the highest abundance differences between the normal and cancerous areas. Only those ion images were selected for which the trend for a given m/z value was similar in all 6 experiments. As judged from generated ion

images 2 adducts have higher average intensities in cancer tissue, and the next 26 ions are of higher intensity in normal tissue. The list of identified compounds is presented in Supplementary Table S2. The identity of some of compounds was confirmed with LIFT[®] MS/MS experiments (Supplementary Table S3). Metabolite mean abundance data from both cancer and normal tissue regions of 28 identified compounds were further subjected to supervised and unsupervised multivariate statistical analysis using the MetaboAnalyst 5.0 online software. The 2D principal components analysis (PCA) score plots of both subsets indicated good separation between the cancer and the normal tissue regions (Fig. 1A).

The best separation of groups was obtained along principal components 1 and 2 (i.e. PC1 and PC2) which accounted for 61.2% and 18.8%, respectively. The separation between the BC and normal tissue samples was further examined using the supervised multivariate statistical analysis - Orthogonal Partial Least Squares Discriminant Analysis (OPLS-DA) (Fig. 1B). We conducted 2000 permutation tests to evaluate the statistical robustness of the OPLS-DA model (Supplementary Fig. S2). Good discrimination was observed between cancer and normal groups ($Q^2 = 0.774$, $R^2Y = 0.998$, P -value < 0.03 (0/2000)). Potential BC biomarkers were selected on the basis of the variable influence on projection (VIP) value resulting from the OPLS-DA model (Fig. 1C). By combining the VIP (> 1.0) with the results from the independent t -test (P -value from t -test < 0.05) and fold change analysis ($0.5 < FC < 1.2$) 10 metabolites were selected as differential for BC tissue and normal samples (Table 1). All data for identified compounds analyzed within this work are presented in Supplementary Table S2.

Next, univariate ROC curve analysis was separately performed to evaluate the diagnostic ability of the models. ROC curves analyses were used to estimate the accuracy of combined signatures model of imaging data. The areas under curves (AUC) of ROC curves were used to determine the diagnostic effectiveness of important metabolites. Applying a ROC approach to biomarker analysis allowed characterization of diagnostic accuracy, and evaluation of the predictive accuracy. The results indicated that all previously selected metabolites have AUC above 0.81 (Table 1). The best ROC analyses with the highest statistical significance were obtained for hypotaurine and 3-methylbutanal (AUC = 0.944, specificity = 1.0 and sensitivity = 0.8). The classification ROC model was based on a random forest algorithm. As shown in Fig. 1D, the combination of levels of 10 selected metabolites was a better discriminator (AUC = 0.993) than each metabolite separately. The results suggest that 10 specific metabolites: glycine, hypotaurine, 3-methylbutanal, ethylphosphate, glutamine, myosmine, PI(22:0/0:0), aminopentanal, proline betaine and methylguanidine could significantly increase the diagnostic potential and serve as useful discriminators of cancer tissues from normal tissues in patients diagnosed with BC. Ion images of all these compounds that differentiate the neoplastic and normal area to the greatest extent are presented in Figs. 2 and 3.

Ion images of 2 amino acids that play essential roles in human tissues were generated and the structure of one of them was confirmed with LIFT MS/MS method. One of the ion images of m/z 98.021 (Fig. 2 A) shows spatial distribution of the $[\text{C}_2\text{H}_5\text{NO}_2 + \text{Na}]^+$ adduct (sodiated glycine). This ion was found to be present at a higher intensity in the normal tissue compared with the cancer tissue. The decreased levels of glycine were observed in lung cancer patients [21] and in serum of BC patients [22]. Similarly, ion assigned to potassium adduct of glutamine (m/z 185.032, Fig. 2 E) was found at a higher intensity in the normal tissue compared to the cancer tissue. NMR-based metabolomics studies have shown the decreased blood levels of glutamine in plasma samples from pancreatic cancer patients [23]. The decrease in the levels of the amino acids discussed above indicates an increased demand for these metabolites for tumor growth. This observation suggests that tumor's biochemistry may be associated with an increased glycolytic flux that has been found to be a major source of respiratory energy for tumor cells, and with the need for increased protein synthesis in tumor cells [24]. It has also been suggested that glycolysis is required to maintain lipogenesis and cholesterogenesis, that are essential for the growth and proliferation of tumor cells [25].

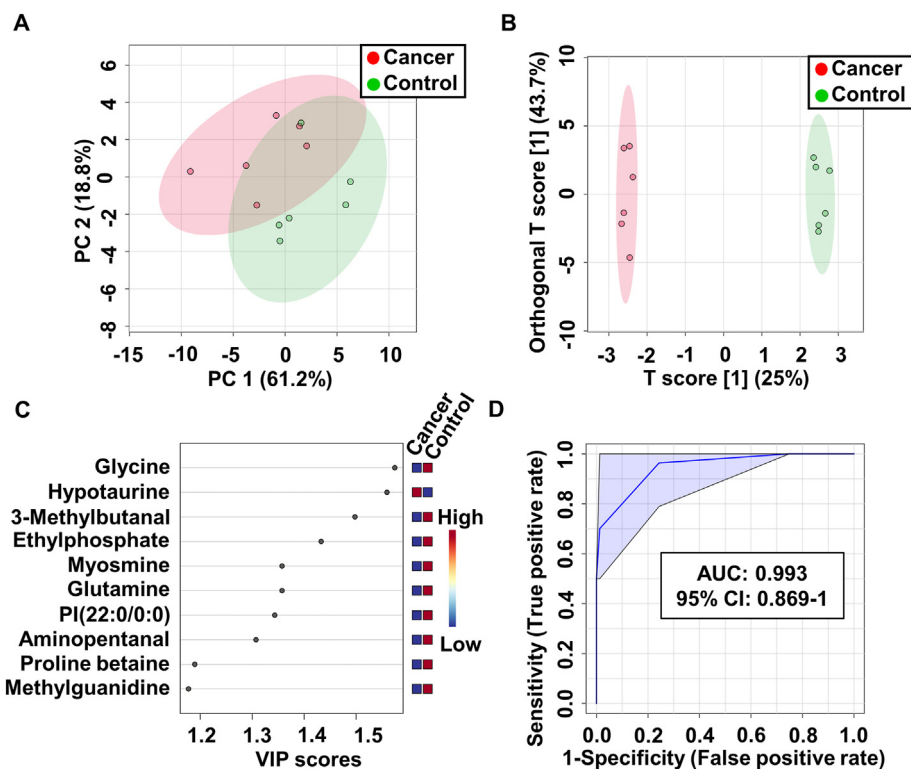


Fig. 1. Metabolomic analysis of tissue samples from bladder cancer (BC) patients. (A) PCA and (B) OPLS-DA scores plots of the cancer (red) and control (green) tissue samples. (C) VIP plot from OPLS-DA analysis. (D) The receiving operator characteristic (ROC) curves for the 10 selected metabolites.

Table 1

Mean metabolite abundance for controls vs. bladder cancer tissues. Bolded metabolites are considered statistically significantly different (P-value <0.05; VIP >1; FC < 0.5 and >1.2) between controls and cancer tissues.

No.	Compound name	Adduct type	m/z^c	P-value ^d	Fold Change ^e	VIP ^f	AUC	Power of the test	
								Sensitivity [%]	Specificity [%]
1	Glycine ^a	[C ₂ H ₅ NO ₂ +Na] ⁺	98.021	0.0025	0.30	1.56	0.92	100	83
2	Hypotaurine ^a	[C ₂ H ₇ NO ₂ S+ ¹⁰⁹ Ag] ⁺	217.924	0.0035	1.39	1.54	0.94	83	100
3	3-Methylbutanal ^a	[C ₅ H ₁₀ O + H] ⁺	87.080	0.0053	0.19	1.47	0.94	83	100
4	Ethylphosphate ^a	[C ₂ H ₇ O ₄ P + K] ⁺	164.971	0.0088	0.30	1.41	0.92	83	83
5	Glutamine ^b	[C ₅ H ₁₀ N ₂ O ₃ +K] ⁺	185.032	0.0147	0.29	1.35	0.92	83	83
6	Myosmine ^b	[C ₉ H ₁₀ N ₂ +H] ⁺	147.092	0.0147	0.29	1.35	0.92	83	83
7	PI(22:0/0:0) ^a	[C ₃₁ H ₆₁ O ₁₂ P+ ¹⁰⁹ Ag] ⁺	765.294	0.0171	0.19	1.32	0.92	100	83
8	Aminopentanal ^b	[C ₅ H ₁₁ NO + H] ⁺	102.091	0.0214	0.39	1.29	0.83	100	67
9	Proline betaine ^a	[C ₇ H ₁₃ NO ₂ +Na] ⁺	166.084	0.0417	0.44	1.17	0.83	100	67
10	Methylguanidine ^a	[C ₂ H ₇ N ₃ +Na] ⁺	96.053	0.0451	0.45	1.16	0.81	67	83

Abbreviations: AUC - area under the curve; FC - fold change; PI - phosphatidylinositol; PS - phosphatidylserine; VIP - variable influence on projection.

^a Putative identification.

^b Identity confirmed with LIFT MS/MS method.

^c Calculated m/z values.

^d P-value determined from Student's t-test.

^e Fold change between cancer and control tissue samples.

^f VIP scores derived from OPLS-DA model.

Moreover, it was found that glycine metabolism is necessary and sufficient for cell transformation and malignancy [26].

In the present study, 11 lipids that play essential roles in the human body showed a large differentiation between neoplastic and normal tissue, and their structures were in some cases successfully confirmed with LIFT MS/MS method (Supplementary Tables S2 and S3). We found, that 5 ions of ¹⁰⁹Ag isotope adducts of phosphoglycerol PG(32:1) (m/z 829.398), phosphoinositol PI(22:0/0:0) (m/z 765.294), phosphoserines PS(O-30:1) (m/z 800.383), PS(30:1) (m/z 814.362), phosphoethanolamine PE(34:4) (m/z 820.388), 4 sodium adducts of diacylglyceride DG(44:1) (m/z 757.668), phosphocholine PC(40:10) (m/z 848.520), phosphoglycerolphosphate PGP(32:1) (m/z 801.471), phosphoethanolamine PE(26:1)

(m/z 628.395), and 2 potassium adducts of phosphoserine PS(36:4) (m/z 822.468), sphingomyeline SM(d18:0/12:0) (m/z 689.499), dominated in the cancer tissue MSI region compared to normal tissue. However, only 1 lipid - PI(22:0/0:0) showed statistically significant differentiation between normal and neoplastic tissues (Fig. 3A). Lipids are the building blocks of cell membranes and play important roles in various biological processes, such as cellular signaling, chemical-energy storage, homeostasis, apoptosis, metabolism, cell adhesion and migration, neurotransmission, signal transduction, vesicular trafficking, post-translational modifications and cell-cell interactions in tissues. These cellular processes are associated with cellular transformations, cancer progression and metastasis. Lipids are linked to cancer at the metabolic level and are expected to be present in

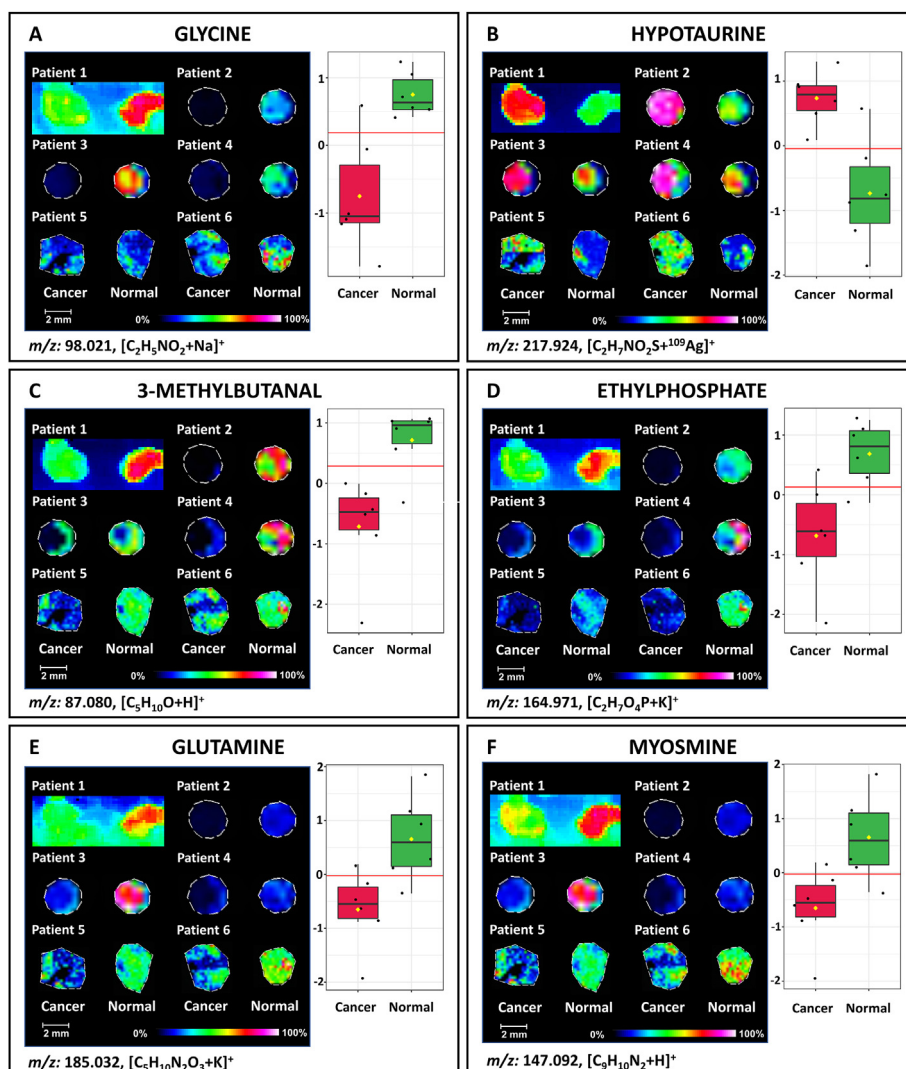


Fig. 2. Results of LDI-MSI analysis of the surface of the bladder cancer (BC) specimens on $^{109}\text{AgNPET}$. The left sides of the individual metabolite panel (A–F) present ion images (TIC normalization) for ions of m/z as stated below each image. The right sides contain plots of distribution of abundance values of metabolite in control and cancer samples with optimal cut-off as a horizontal dashed line. All ion images are within $\pm 0.05 m/z$.

cancer cells, tissues and biofluids. Multiple studies have demonstrated altered lipid profiles in biological samples that have been screened to identify biomarkers in cancer research [27,28]. Several reports have shown the spatial distributions of many potential lipid-based biomarkers in various malignant tumors such as lung [29], breast [30], ovarian [31], colorectal [32], prostate [33], kidney [34], renal [35], bladder [36] and thyroid cancers [37]. Dill et al. [38] demonstrated distributions of the multiple lipids and free fatty acids species between cancerous and noncancerous dog bladder tissue samples with desorption electrospray ionization MS (DESI-MS). The same group of researchers in another study used human BC tissue samples to visualize of glycerophospholipid (GP) distribution in cancerous and normal tissue. They found that tumor tissue shows increased intensities for different GPs such as phosphatidylserine (PS) and phosphatidylinositol (PI) when compared to the normal tissue [36]. Wittman et al. [39], measured multiple distinct compounds in human urine samples, that differentiate BC from non-cancer controls. They selected 25 potential biomarkers related to lipid metabolism.

Ion assigned to proton adduct of 3-methylbutanal (m/z 87.080; Fig. 2C) was found in higher intensity in normal tissue compared to cancer tissue. 3-Methylbutanal also known as isovaleraldehyde is an aldehyde that occurs naturally in all eukaryotes. In humans, this compound has been found to be associated with several diseases. Previous

research revealed significantly reduced level of 3-methylbutanal in urine samples from patients with clear cell renal cell carcinoma which may be associated with higher level of aldehyde dehydrogenase that converts aldehydes to their respective carboxylic acids and is often upregulated in cancer [40]. Furthermore, in the human lung cancer cell line, 3-methylbutanal was found at decreased concentrations [41].

One of the ion images of m/z 166.084 (Fig. 2C) shows spatial distribution of the sodium adduct of proline betaine. This secondary metabolite has been described previously as a highly effective osmoprotectant in many plants. In humans, proline betaine was at reduced levels in plasma samples from patients with esophageal squamous cell carcinoma compared to healthy controls which is also in line with our results [42]. Similar results were obtained in metabolomic analysis of serum samples from patients with preeclampsia [43]. Proline betaine was found to be up-regulated in urine samples from patients with uterine cervix cancer and renal cell carcinoma [44,45].

The MSI results of the bladder tissue imprint suggest, that the ion of m/z 96.053 (Fig. 3 D) corresponds to sodiated adduct of methylguanidine which was found in higher abundance in normal tissue. Methylguanidine is an organic compound containing a guanidine moiety in which one of the amino hydrogens is substituted by a methyl group. Endogenous methylguanidine is produced by conversion from creatinine and some

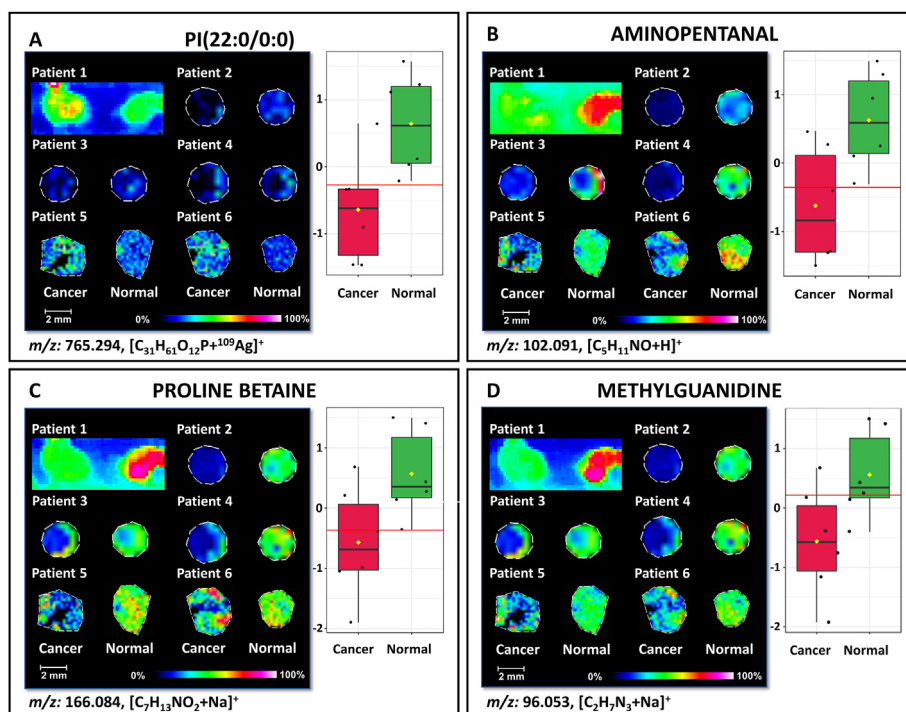


Fig. 3. Results of LDI-MSI analysis of the surface of the bladder cancer (BC) specimens on $^{109}\text{AgNPET}$. (A–D) The left sides of the individual metabolite panel (A–D) present ion images (TIC normalization) for ions of m/z as stated below each image. The right sides contain plots of distribution of abundance values of metabolite in control and cancer samples with optimal cut-off as a horizontal dashed line. All ion images are within $\pm 0.05 m/z$.

amino acids [46]. Previous studies reported the potential toxicity of methylguanidine [47]. Methylguanidine was proposed as a serum potential biomarker of pancreatic cancer based on LC/GC–MS analyses which revealed a higher abundance of this compound in serum of patients with this tumor compared to controls [48]. Higher level of methylguanidine was also observed in serum of patients with cholangiocarcinoma [49]. This metabolite was identified in higher concentration in urine samples from patients with chronic pancreatitis by NMR-based metabolomics [50]. Significantly increased level of methylguanidine was identified in urine samples from dogs with BC compared to controls in an NMR-based metabolomics study [51].

Ion images presenting higher average intensity in the area of normal tissue were recorded for proton adduct of myosmine (m/z 147.092; Fig. 2F). Myosmine is a derivative of pyridines which can be found in tobacco and in various foods. It is suspected that this compound may be related to esophageal cancer [52]. Ion assigned to potassium adduct of ethylphosphate (m/z 164.971; Fig. 2D) was found in higher intensity in normal tissue compared to cancer tissue. Ethylphosphate is an organic compound that belongs to the class of monoalkyl phosphates. This compound was identified in human saliva by LC-MS [53]. Also, the ion of m/z 102.091 (Fig. 3B) was found in higher abundance in normal tissue and was assigned to $[\text{M}+\text{H}]^+$ adduct of aminopentanal.

Ion image that shows higher intensity in the area of cancer tissue has been created for the m/z 217.924 which corresponds to the ^{109}Ag adduct of hypotaurine (Fig. 2B). Hypotaurine is a sulfonic acid that is an intermediate in the biosynthesis of taurine from cysteine sulphonic acid. Previous research has established that hypotaurine has antioxidant properties *in vivo* [54] and also acts as a neurotransmitter [55]. Previously, using ^1H NMR, hypotaurine was found in increased level in serum samples of BC patients resistant to neoadjuvant chemotherapy [56]. Elevated level of hypotaurine was found in saliva of patients with medication-related osteonecrosis of the jaw [57]. In addition, hypotaurine was found to be upregulated in tissue of patients with colorectal cancer and related to the progression of this tumor [58].

4.2. Pathway analysis

A metabolic pathway impact analysis was performed to identify the most relevant pathways involved in the observed changes of tissue metabolite levels. Ten most significant metabolites were subjected to pathway analysis and quantitative pathway enrichment analysis. Three of them were found to be relevant to human metabolism (Table 2). Seventeen metabolic pathways i.e., glyoxylate and dicarboxylate metabolism, aminoacyl-tRNA biosynthesis, D-glutamine and D-glutamate metabolism, nitrogen metabolism, taurine and hypotaurine metabolism, arginine biosynthesis, glutathione metabolism, alanine, aspartate and glutamate metabolism, porphyrin and chlorophyll metabolism, glycine, serine and threonine metabolism, pyrimidine metabolism, primary bile acid biosynthesis, purine metabolism, mercaptopurine action pathway, thioguanine action pathway, azathioprine action pathway and mercaptopurine metabolism pathway, were found to be significantly impacted when comparing BC to normal tissue. Results from pathway impact analysis are shown in Supplementary Tables S3 and S4. Glycine,

Table 2

Selected metabolites and their involvement in different pathways.

Compound name	Pathway involved
Glycine	Glyoxylate and dicarboxylate metabolism, aminoacyl-tRNA biosynthesis, glutathione metabolism, porphyrin and chlorophyll metabolism, glycine, serine and threonine metabolism, primary bile acid biosynthesis, mercaptopurine action pathway, thioguanine action pathway, azathioprine action pathway
Glutamine	Glyoxylate and dicarboxylate metabolism, aminoacyl-tRNA biosynthesis, D-glutamine and D-glutamate metabolism, nitrogen metabolism, arginine biosynthesis, alanine, aspartate and glutamate mercaptopurine action pathway metabolism, pyrimidine metabolism, purine metabolism, thioguanine action pathway, azathioprine action pathway, mercaptopurine metabolism pathway
Hypotaurine	Taurine and hypotaurine metabolism

glutamine and hypotaurine were found to be involved in these metabolic pathways (Table 2). These pathways are well known to be related to cancer, e.g. taurine and hypotaurine metabolism have been shown to be related to BC [59,60] and renal cell carcinoma [61], sulfur metabolism has been shown to be related to breast cancer [62], and aminoacyl-tRNA biosynthesis pathway has been shown to be related to prostate cancer [63].

4.3. Diagnostic value of nanoparticles for MSI of cancer tissues

The diagnosis of most cancers is based on a molecular pathology that is currently most often performed by immunohistochemical analysis (IHC) or fluorescence *in situ* hybridization (FISH) which most often uses macromolecules such as proteins or nucleic acids of varying lengths [64, 65]. These methods are complex, time-consuming, and require specialized and expensive antibodies or labeling. Surgical excision of the bladder tumor is currently a method of choice for treating patients suffering from BC, therefore it is important to quickly and precisely define the neoplastic tissue border during surgery in order to completely remove the tumor without damaging normal tissue. Numerous previous studies have shown that metabolites enable a more precise determination of pathology and may serve as potential diagnostic biomarkers in a variety of malignancies [66]. The use of MSI allows not only to identify potential tumor biomarkers but also to determine their location on the surface of the examined tissue. Nowadays almost all of MSI is made with the use of MALDI with many of its drawbacks including (i) abundant and numerous chemical background peaks in the low-mass region ($m/z < \approx 1000$) due to the presence of the applied matrix; (ii) the frequent need for external mass calibration; (iii) low mass resolution and accuracy due to the thickness of the tissue samples; (iv) low ionization efficiency for many organic compounds present in the samples in their non-charged states; (v) inhomogeneous matrix crystallization; and (vi) commonly observed acid-catalyzed hydrolysis of various biomolecules, and thus it is not suitable for metabolites. On the other hand, some nanoparticles such as silver and gold-based lacks most of above mentioned MALDI drawbacks and are one of the most interesting choices for studying of differentiation between cancer and normal tissues.

5. Conclusion

In this study, LDI-MSI technique with the use of nanoparticle-enhanced SALDI-type $^{109}\text{AgNPET}$ target was used for MSI of human bladder tissue. Ion images produced for few dozens of compounds of interest presented attention-grabbing differentiation of intensities. Univariate and multivariate statistical analyses revealed 10 metabolites that differentiated cancer from normal tissues. Among these metabolites, glycine, 3-methylbutanal, ethylphosphate, glutamine, myosmine, PI(22:0/0:0), aminopentanal, proline betaine and methylguanidine were found in higher abundance in normal tissue samples and hypotaurine was found at a higher level in cancer tissue samples. These compounds may significantly increase diagnostic potential and serve as useful discriminators of cancerous versus normal tissues in patients diagnosed with BC. Published results demonstrate that nanoparticle-based LDI-MSI must be considered as a powerful tool for analysis of biological objects and especially for biomarker discovery.

Financial disclosure

This work was supported by the National Science Centre (NCN), SONATA grant no. UMO-2018/31/D/ST4/00109.

The author contributions

Study design: Krzysztof Ossoliński Tomasz Ruman, Joanna Nizioł.

Data collection: Joanna Nizioł, Adrian Arendowski, Aneta Plaza-Altamer, Krzysztof Ossoliński, Anna Ossolińska, Tadeusz Ossoliński.

Statistical Analysis: Joanna Nizioł.

Data interpretation: Joanna Nizioł, Tomasz Ruman.

Manuscript preparation: Joanna Nizioł, Krzysztof Ossoliński, Artur Kołodziej, Tomasz Ruman.

Literature Search: Joanna Nizioł, Krzysztof Ossoliński.

Funds Collection: Joanna Nizioł.

Declaration of competing interest

The authors declare no conflict of interests.

Acknowledgements

Mr Dominik Ruman is acknowledged for creating MS search engine of chemical compounds.

Appendix A. Supplementary data

Supplementary data to this article can be found online at <https://doi.org/10.1016/j.advms.2022.12.002>.

References

- [1] Sung H, Ferlay J, Siegel RL, Laversanne M, Soerjomataram I, Jemal A, et al. Global cancer statistics 2020: GLOBOCAN estimates of incidence and mortality worldwide for 36 cancers in 185 countries. *CA A Cancer J Clin* 2021;71:209–49. <https://doi.org/10.3322/CAAC.21660>.
- [2] Kamat AM, Hegarty PK, Gee JR, Clark PE, Svatek RS, Hegarty N, et al. ICUD-EAU international consultation on bladder cancer 2012: screening, diagnosis, and molecular markers. *Eur Urol* 2013;63:4–15. <https://doi.org/10.1016/J.EURURO.2012.09.057>.
- [3] González de Vega R, Clases D, Fernández-Sánchez ML, Eiró N, González LO, Vizoso FJ, et al. MMP-11 as a biomarker for metastatic breast cancer by immunohistochemical-assisted imaging mass spectrometry. *Anal Bioanal Chem* 2019;411:639–46. <https://doi.org/10.1007/s00216-018-1365-3>.
- [4] Paine MRL, Kooijman PC, Fisher GL, Heeren RMA, Fernández FM, Ellis SR. Visualizing molecular distributions for biomaterials applications with mass spectrometry imaging: a review. *J Mater Chem B* 2017;5:7444–60. <https://doi.org/10.1039/C7TB01100H>.
- [5] Steurer S, Singer JM, Rink M, Chun F, Dahlem R, Simon R, et al. MALDI imaging-based identification of prognostically relevant signals in bladder cancer using large-scale tissue microarrays. *Urol Oncol Semin Orig Investig* 2014;32:1225–33. <https://doi.org/10.1016/J.UROLONC.2014.06.007>.
- [6] Ifa DR, Wiseman JM, Song Q, Cooks RG. Development of capabilities for imaging mass spectrometry under ambient conditions with desorption electrospray ionization (DESI). *Int J Mass Spectrom* 2007;259:8–15. <https://doi.org/10.1016/J.IJMS.2006.08.003>.
- [7] Sekula J, Nizioł J, Rode W, Ruman T. Gold nanoparticle-enhanced target (AuNPET) as universal solution for laser desorption/ionization mass spectrometry analysis and imaging of low molecular weight compounds. *Anal Chim Acta* 2015;875:61–72. <https://doi.org/10.1016/J.ACA.2015.01.046>.
- [8] Nizioł J, Rode W, Zieliński Z, Ruman T. Matrix-free laser desorption–ionization with silver nanoparticle-enhanced steel targets. *Int J Mass Spectrom* 2013;335:22–32. <https://doi.org/10.1016/J.IJMS.2012.10.009>.
- [9] Nizioł J, Rode W, Laskowska B, Ruman T. Novel monoisotopic $^{109}\text{AgNPET}$ for laser desorption/ionization mass spectrometry. *Anal Chem* 2013;85:1926–31. <https://doi.org/10.1021/ac303770y>.
- [10] Nizioł J, Ruman T. Surface-transfer mass spectrometry imaging on a monoisotopic silver nanoparticle enhanced target. *Anal Chem* 2013;85. <https://doi.org/10.1021/ac4031658>.
- [11] Nizioł J, Ossoliński K, Ossoliński T, Ossolińska A, Bonifay V, Sekula J, et al. Surface-Transfer mass spectrometry imaging of renal tissue on gold nanoparticle enhanced target. *Anal Chem* 2016;88. <https://doi.org/10.1021/acs.analchem.6b01859>.
- [12] Arendowski A, Nizioł J, Ossoliński K, Ossolińska A, Ossoliński T, Dobrowski Z, et al. Laser desorption/ionization MS imaging of cancer kidney tissue on silver nanoparticle-enhanced target. *Bioanalysis* 2018;10:83–94. <https://doi.org/10.4155/bio-2017-0195>.
- [13] Moch H, Cubilla AL, Humphrey PA, Reuter VE, Ulbright TM. The 2016 WHO classification of tumours of the urinary system and male genital organs—Part A: renal, penile, and testicular tumours. *Eur Urol* 2016;70:93–105. <https://doi.org/10.1016/J.EURURO.2016.02.029>.
- [14] Sauter G, Algaba F, Amin MB, Busch C, Chevillet J, Gasser T, et al. Tumours of the urinary system: non-invasive urothelial neoplasias. In: WHO classification of classification of tumours of the urinary system and male genital organs. IARCC Press Lyon; 2004. p. 89–157.
- [15] Suckau D, Resemann A, Schuereberg M, Hufnagel P, Franzen J, Holle A. A novel MALDI LIFT-TOF/TOF mass spectrometer for proteomics. *Anal Bioanal Chem* 2003;376:952–65. <https://doi.org/10.1007/s00216-003-2057-0>.

